Available online at www.sciencedirect.com

ScienceDirect

Proceedings of the Combustion Institute 39 (2023) 1515–1524

Proceedings of the Combustion Institute

www.elsevier.com/locate/proci

Effects of low-temperature chemical reactions on ignition kernel development and flame propagation in a DME-air mixing layer

Yiqing Wang [a], Wang Han [b,c], Thorsten Zirwes [d,e], Feichi Zhang [d], Henning Bockhorn [d], Zheng Chen [a,*]

[a] *SKLTCS, CAPT, BIC-ESAT, College of Engineering, Peking University, Beijing 100871, China*
[b] *School of Astronautics, Beihang University, Beijing 100191, China*
[c] *Aircraft and Propulsion Laboratory, Ningbo Institute of Technology, Beihang University, Ningbo 315800, China*
[d] *Engler-Bunte-Institute, Karlsruhe Institute of Technology, Karlsruhe 76131, Germany*
[e] *Steinbuch Centre for Computing (SCC), Karlsruhe Institute of Technology, Karlsruhe 76131, Germany*

Received 4 January 2022; accepted 2 July 2022
Available online 25 July 2022

Abstract

The impact of chemical reactions at low-temperature (i.e., low-temperature chemistry, LTC) and LTC-induced cool flames on autoignition and premixed flame propagation has been investigated extensively. However, much less analysis is made to explore the role of LTC in forced ignition of non-premixed fuel/oxidizer systems. The objective of this work is to assess and interpret the effects of LTC on ignition kernel development and subsequent flame transition in a quiescent DME-air mixing layer. A series of two-dimensional simulations are conducted for forced ignition by a hot spot. It is found that under elevated initial temperatures and pressures, a cool flame or a warm flame can be directly ignited depending on the hot spot temperature T_{ig}. When T_{ig} is relatively low, a three-staged ignition process is observed where the cool, warm and hot flames are initiated sequentially. A novel penta-brachial flame structure is identified consisting of a trailing warm flame and a trailing cool flame attached to the hot triple flame. A parametric study is conducted to examine the effects of mixture layer thickness and hot spot size and location on ignition kernel development. It is found that the mixture layer thickness has little influence on the cool flame initiation but it substantially affects the subsequent warm flame or hot flame initiation. It is demonstrated that the mixture fraction range covered by the hot spot has a strong impact on subsequent flame initiation. Moreover, different ignition modes (e.g., ignition failure, only hot flame initiation and only cool flame initiation) can be achieved via changing the hot spot configuration. Furthermore, the analysis of cool flame displacement speed indicates that the cool flame initiated by the hot spot is a self-sustained partially premixed flame. Its density-weighted displacement speed

* Corresponding author.
E-mail address: cz@pku.edu.cn (Z. Chen).

https://doi.org/10.1016/j.proci.2022.07.024

changes linearly with flame stretch. These results provide useful insights into how LTC affects non-premixed ignition.

Keywords: Ignition; Mixing layer; Low temperature chemical reactions; Cool flame; Flame propagation

1. Introduction

For large hydrocarbon fuels, chemical reactions at low-temperature (i.e., low-temperature chemistry, LTC) and LTC-induced cool flames have great impact on ignition control in high-efficiency, low-emission engines, such as homogeneous charge compression ignition (HCCI) engines, spark assistant compression ignition (SACI) engines and gas turbines [1]. Besides, cool flame properties can serve as important targets to validate the LTC in kinetic models. In this context, considerable effort has been devoted to understanding the effects of LTC on ignition and flame propagation under autoignition conditions where a cold fuel mixes with a hot oxidizer [2–6].

However, there are only a few studies investigating the role of LTC in forced ignition of premixed or non-premixed flames. It was found that a cool flame can be directly initiated in a dimethyl ether (DME)/air mixture by a hot spot [7] or a hot particle [8] at a proper temperature that only triggers LTC. These studies showed that the premixed cool flame can substantially accelerate the subsequent hot flame initiation and propagation, leading to a double-flame structure with coexisting premixed cool and hot flames. Yang and Zhao [9] found that at elevated temperatures, the minimum ignition energy (MIE) for premixed cool flames is much lower than that for hot flames. These studies [7–9] considered premixed reactants and clearly demonstrated that LTC has a large impact on forced ignition of premixed flames. However, the effects of LTC on forced ignition of non-premixed mixtures receive little attention and are still not well understood. This motivates the current work.

The forced ignition of non-premixed fuel/oxidizer systems is a fundamental research topic and has broad applications [10]. Due to the inhomogeneity in mixture composition, the ignition outcome is very sensitive to the position of the spark/hot spot [11–15]. Successful ignition in a mixing layer between fuel and oxidizer can generate triple flames propagating along the stoichiometric mixture fraction surface [16]. The dynamics of triple flames is closely related to the stabilization of turbulent diffusion flames and thereby has received considerable attention. Im and Chen [17] numerically investigated the transient evolution of a hydrogen triple flame and its interaction with a vortex. Owston and Abraham [18,19] assessed the effects of ignition position and mixing layer thickness on the initiation of hydrogen triple flames. The above studies mainly focused on the initiation of triple flames while the minimum ignition energy (MIE) was not investigated. Pearce and Daou [20] quantified the MIE for triple flame ignition in a quiescent mixing layer. More recently, Xie et al. [21] assessed the effects of strain rate and Lewis number on the ignition kernel development and MIE for forced ignition of laminar counterflow diffusion flames. In all studies mentioned above [10–21], either one-step chemical reactions or simple fuels such as hydrogen and methane were considered; only few studies considered large hydrocarbon fuels, e.g. propane [22] and n-heptane [23]. To our knowledge, currently there is no study on how LTC and cool flames affect the forced ignition of non-premixed mixtures.

Based on the above-mentioned considerations, the objective of this study is to investigate how LTC influences the forced ignition in a mixing layer between dimethyl ether (DME) and air. Specifically, the following three questions shall be answered: (1) what are the conditions under which a cool flame can be directly ignited in a mixing layer? (2) how is the cool flame transformed into the canonical hot flame? and (3) what are the cool flame characteristics? To answers these questions, we conduct a series of two-dimensional simulations for forced ignition in a quiescent DME-air mixing layer. This idealized configuration without complicated flow conditions (e.g., turbulence) is employed in order to isolate and quantify the impact of LTC. DME is considered in this work since it is a promising alternative fuel and has well-established, compact kinetic mechanism.

2. Model and numerical methods

Two-dimensional simulations are conducted for the transient ignition processes occurring in a quiescent DME-air mixing layer. The configuration is axisymmetric and thereby is studied in a cylindrical coordinate system as shown in Fig. 1.

Figure 1 shows that the mixing layer is horizontally centered at z=0 mm, with pure DME and air on the top and bottom sides, respectively. The initial distribution of mixture fraction Z is given by:

$$Z = [1 - erf(4z/\delta)]/2, \quad (1)$$

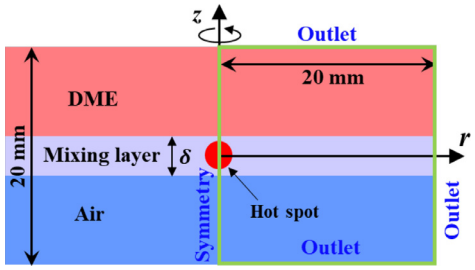

Fig. 1. The schematic of the DME-air mixing layer ignited by a hot spot. The green square represents the computational domain. The boundary conditions are indicated. (For interpretation of the references to colour in this figure legend, the reader is referred to the web version of this article.)

where erf is the error function and δ characterizes the mixing layer thickness. The distribution of species mass fraction Y_k along the z direction is given as:

$$Y_k = Z * Y_{k,F} + (1 - Z) * Y_{k,O}, \tag{2}$$

where $Y_{k,F}$ and $Y_{k,O}$ are the mass fractions of kth species on the DME and air sides. Note that $Y_k = 0$ for all other species except DME, O_2 and N_2. The gas in the domain is initially quiescent at temperature, T_0, and pressure, P_0, to be specified later.

A spherical hot spot with the radius of r_{ig} and temperature of T_{ig} is placed on the symmetry axis. Previous studies showed that cool flame initiation relies on the hot spot temperature [7,8] or energy [9]. Therefore, the hot spot temperature, T_{ig} is varied ranging from 800 K to 3200 K in order to identify multiple ignition modes. The mixing layer thickness, δ=2 mm, and hot spot radius, r_{ig}=0.5 mm, are used as a baseline case unless otherwise specified.

The transient ignition process is simulated using the in-house solver developed based on OpenFOAM [24,25]. It solves the compressible balance equations for multi-component reactive flows using the finite volume method. The mixture-averaged transport model is adopted. The oxidation of DME is modeled by a skeletal mechanism [26] which includes both LTC and high-temperature chemistry (HTC). This mechanism was validated and widely used in previous studies [7–9]. The LTC for DME was discussed in details in previous studies [1,8]. The reaction rates, diffusion coefficients and thermo-physical properties are calculated by Cantera [27]. Detailed descriptions of the governing equations and numerical methods can be found in [25]. The computational domain, which is a wedge with 1 ° opening angle, and boundary conditions are depicted in Fig. 1. A uniform mesh with the cell size of $\Delta r = \Delta z$=33 μm is used and grid convergence is ensured (see section S1 in Supplementary Material). Buoyancy is not considered because the focus lies on identifying the effect of LTC.

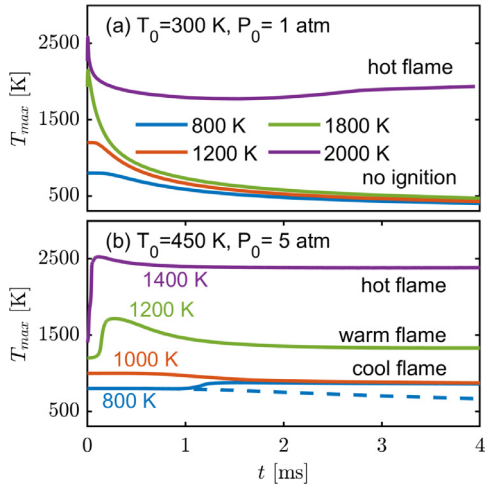

Fig. 2. Temporal evolution of maximum temperature $T_{\max}$ for different hot spot temperatures, T_{ig}: (a) T_0=300 K, P_0=1 atm and (b) T_0=450 K, P_0=5 atm. The dashed line represents the results when the LTC is excluded.

3. Results and discussions

3.1. Cool flame ignition in a mixing layer

We first study the conditions under which a cool flame can be directly ignited. Different initial temperatures and pressures, T_0 and P_0, and different hot spot temperatures, T_{ig}, are tried to ignite cool, warm and hot flames. The typical results are shown in Fig. 2, which plots the temporal evolution of maximum temperature within the whole domain, $T_{\max}$. At normal temperature and pressure (NTP) with $T_0 = 300$ K and $P_0 = 1$ atm, a hot flame can be successfully ignited for $T_{ig} = 2000$ K, while ignition fails for $T_{ig} \leq 1800$ K. Therefore, there exists a critical hot spot temperature, T_c, between 1800 K and 2000 K, above which successful ignition can be achieved. This is similar to the concept of MIE for non-premixed ignition studied in [20,21] where the LTC is not considered. Moreover, Fig. 2a demonstrates that cool flame cannot be initiated under NTP.

However, at elevated temperature and pressure of $T_0 = 450$ K and $P_0 = 5$ atm, different types of flames can be ignitied by changing T_{ig}, as shown in Fig. 2b. For $T_{ig} = 1400$ K, a hot flame is initiated directly. For $T_{ig} = 1200$ K, the ignition kernel cannot develop into a hot flame, but finally maintains a temperature of 1300–1400 K, indicating the formation of a warm flame characterized by the intermediate flame temperature around 1400 K (details on warm flames can be found in [1]). For lower hot spot temperature of $T_{ig} = 1000$ K or 800 K, a warm flame cannot be ignited, while a cool flame is successfully initiated and $T_{\max}$ reaches a steady value at

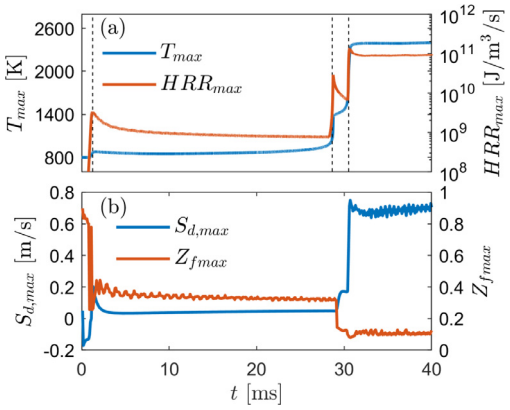

Fig. 3. Temporal evolution of (a) $T_{\max}$ and $\mathrm{HRR}_{\max}$ and (b) $S_{d,\max}$ and $Z_{f,\max}$ for T_{ig}=800 K, T_0=450 K and P_0=5 atm.

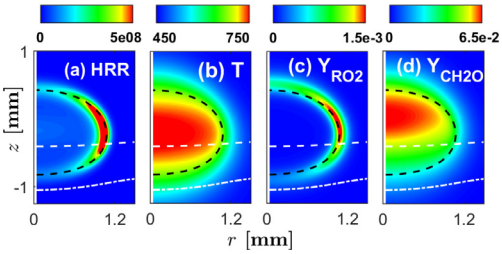

Fig. 4. Contours of HRR, T and mass fractions of $CH_3OCH_2O_2$ and CH_2O at t=20 ms for the same case considered in Fig. 3. The white dashed and dash-dotted lines are the iso-lines for Z=0.3 and Z_{st}=0.1, respectively. The black dashed lines are the iso-lines of T=750 K. These dashed lines are also plotted in the following contour plots.

around 900 K. When the LTC is excluded from the kinetic model, ignition fails for $T_{ig} = 800$ K (see the dashed line in Fig. 2b). This further demonstrates that the cool flame with $T_{\max}$ being around 900 K is caused by LTC.

The above results suggest that under elevated temperature and pressure conditions, a cool flame or a warm flame can be directly initiated in the DME-air mixing layer when the hot spot temperature is within a certain range. Note that we also use an energy source term to model the "hot spot" and similar results are obtained (see section S2 in Supplementary Material). The flame structures will be further examined in the following subsections.

3.2. Transition among cool, warm and hot flames

After the LTC-controlled cool flame is ignited, HTC takes place in the burnt gas of the cool flame and eventually a hot flame is ignited. The transition process from a cool flame to a hot flame is investigated in this subsection. Figure 3a shows the evolution of the maximum temperature, $T_{\max}$, and maximum heat release rate, $\mathrm{HRR}_{\max}$, during the transient ignition process for $T_{ig} = 800$ K, $T_0 = 450$ K and $P_0 = 5$ atm. A three-staged ignition process is clearly observed, which is identified by three peaks of $\mathrm{HRR}_{\max}$ as well as three sharp increments in $T_{\max}$ (see dashed lines in Fig. 3a). Figure 4 plots the contours of HRR, temperature and mass fractions of $CH_3OCH_2O_2$ (RO_2) and CH_2O at t=20 ms. The cool flame front is represented by the iso-line of T=750 K, which is seen to fall within the high HRR and Y_{RO_2} regions (see black dashed lines in Fig. 4a and c). These results demonstrate that the cool flame features small HRR, low flame temperature, RO_2 radical pool and accumulation of CH_2O. This is consistent with previous studies [1,7]. Moreover, it is observed that the cool flame shows a quasi-ellipsoid shape without a diffusion flame branch and is located fully above the stoichiometric plane (Z_{st}=0.1, denoted by the white dash-dotted line in Fig. 4), which is intrinsically different from the canonical hot triple flame. In addition, the HRR in the flame tip is much higher than that in the two wings, indicating the cool flame mainly propagates in the horizontal direction through the mixing layer.

To quantify the cool flame propagation, the analysis on displacement speed S_d based on temperature field is applied. Equation (3) is the conservation equation for temperature:

$$\rho C_p \frac{DT}{Dt} = \omega_T' + \frac{Dp}{Dt} + \nabla \cdot (\lambda \nabla T) - \left(\rho \sum_{k=1}^{N} C_{p,k} Y_k \vec{V}_k\right) \cdot \nabla T, \tag{3}$$

where ρ is density, C_p the heat capacity of the mixture at constant pressure, p the pressure, ω_T' the heat release rate, λ the thermal conductivity, $C_{p,k}$ heat capacity of the species k at constant pressure, Y_k the mass fraction of species k, $\vec{V}_k$ the diffusion speed of species k and N the number of species. D represents the material derivative. Note that the stress tensor term is not shown here.

From the LHS of Eq. (3), S_d determined on the iso-line of T=750 K is defined as:

$$S_d = \frac{1}{|\nabla T|}\frac{DT}{Dt} = \frac{1}{|\nabla T|}\frac{\partial T}{\partial t} + \vec{u} \cdot \frac{\nabla T}{|\nabla T|}, \tag{4}$$

where $\vec{u}$ is the flow velocity. Figure 3b shows the temporal evolutions of S_d and Z at the location of maximum S_d, i.e. $S_{d,\max}$ and $Z_{f,\max}$. It is seen that similar to $T_{\max}$ and $\mathrm{HRR}_{\max}$, $S_{d,\max}$ and $Z_{f,\max}$ also exhibit a three-staged evolution. In the cool flame stage ($2< t <28$ ms), both $S_{d,\max}$ and $Z_{f,\max}$ reach a quasi-steady state after a short duration. The cool flame sustainably propagates at a very low speed along the iso-contours of Z=0.3 (denoted by the white dashed line in all contours). Note that Z=0.3 is approximately the most reactive mixture fraction where the first-stage ignition delay time is the shortest for DME-air mixtures at

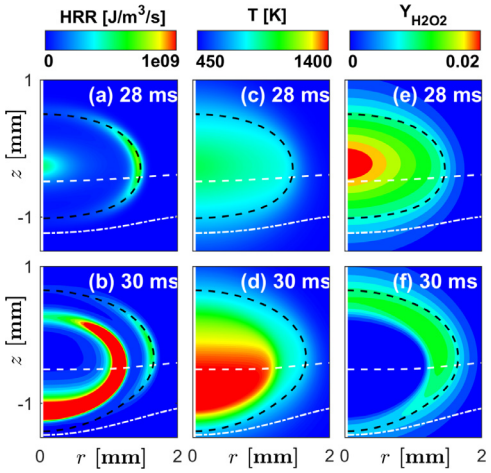

Fig. 5. Contours of HRR, T and mass fraction of H_2O_2 during warm flame initiation and propagation. The upper and lower rows are for $t = 28$ ms and 30 ms, respectively.

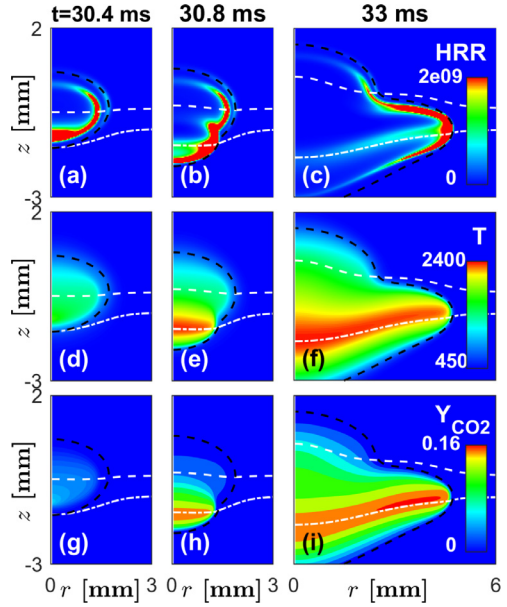

Fig. 6. Contours of HRR, T and mass fraction of CO_2 during hot flame initiation and propagation.

T_0=800 K and P_0=5 atm. Once the warm flame is initiated at 28< t <30 ms, $S_{d,\max}$ jumps to a higher value while an opposite trend is observed for $Z_{f,\max}$. Figure 3b shows that the warm flame evolves into a hot flame in a very short time, and that $S_{d,\max}$ further increases and finally reaches a large value around of 0.7 m/s. Meanwhile, $Z_{f,\max}$ decreases to the stoichiometric mixture fraction (i.e., Z_{st}=0.1) as expected.

To understand the evolution of the warm flame, the contours of HRR, T and mass fractions of H_2O_2 during the warm flame initiation are plotted in Fig. 5. At t=28 ms, a local peak of HRR is first initiated at the center of the burned products of the cool flame, where the maximum T and $Y_{H_2O_2}$ appear. Large amount of H_2O_2 is preferably formed by intermediate-temperature chemical reactions (ITC) [1] and thus contributes to the generation of warm flame. Figure 5b shows that at t=30 ms, a quasi-spherical warm flame is fully initiated and it propagates outwardly, leading to a double-flame structure of both cool and warm flames. During this process, the accumulated H_2O_2 is consumed by the warm flame (see Fig. 5f) and the burnt gas temperature is increased to 1400 K (see Fig. 5d).

The warm flame has very short duration and it quickly evolves into a hot flame. This process is shown in Fig. 6. At t=30.4 ms, the lower branch of warm flame first reaches the stoichiometric plane, which is favored by HTC. Therefore, a hot flame is ignited immediately at the intersection between the warm flame front and the stoichiometric plane, and then a typical triple flame structure is formed at t=30.8 ms. A large amount of CO_2 is produced by the hot diffusion flame branch. The whole hot triple flame propagates along the stoichiometric plane (Z_{st}=0.1, the dash-dotted lines in Fig. 6) at a much faster speed than the warm and cool flames. Finally, the rich premixed hot flame branch catches up and merges with the leading warm and cool flames. However, due to the wider flammability of cool and warm flames, they are only partially engulfed by the rich premixed hot flame branch, resulting in a trailing warm flame and a trailing cool flame attached to the rich premixed hot flame branch in the very rich region at t=33 ms. To the best of our knowledge, such penta-brachial flame structure is observed for the first time. Note that the warm flame branch is smoothly connected with the rich premixed hot flame branch. In addition, as shown in Fig. 7, the trailing warm and cool flames can still be observed even for T_{ig}=1400 K (see Fig. 7a), at which the hot flame is directly ignited (see Fig. 2b). In contrast, when LTC is not included, the top trailing cool flame branch disappears (see Fig. 7b). This indicates that the penta-brachial flame structure is an essential characteristic induced by LTC and ITC and is independent of the properties of the hot spot. On the other hand, it can be seen from our simulations (e.g., Fig. 3) that once the penta-branch flame structure is fully developed, the flame propagates without any noticeable change in flame speed or flame morphology, indicating that this penta-branch flame has reached a quasi-steady state.

The above results indicate that after the cool flame is ignited, the warm and hot flames can be subsequently triggered by ITC and HTC, respectively. Due to the difference in their propagation speeds, transition among these flames is observed.

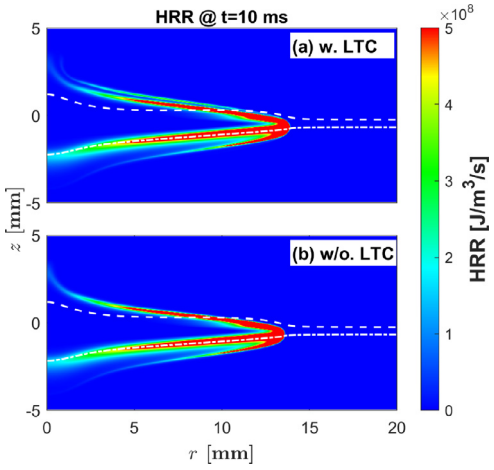

Fig. 7. Flame structures at t=10 ms for the cases with LTC and without LTC. T_{ig}=1400 K. T_0=450 K, P_0=5 atm and δ=2 mm.

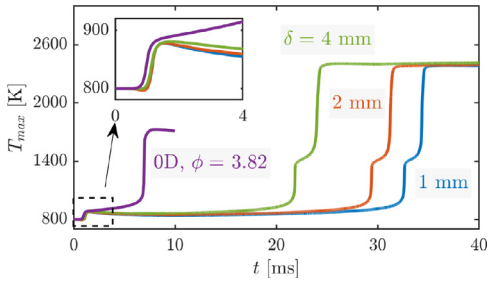

Fig. 8. The temporal evolution of $T_{\max}$ for different δ at T_{ig}=800 K, T_0=450 K and P_0=5 atm. The result for 0D homogeneous ignition with ϕ=3.82 is also shown.

3.3. Parametric study on ignition process

A parametric study is conducted here to examine whether the above results are sensitive to the mixing layer thickness δ, hot spot radius r_{ig} and its location. These parameters are of practical relevance and were shown to affect non-premixed ignition [11,13,18].

The effects of δ on the ignition process are shown in Fig. 8, which compares the results for three mixing layer thicknesses of δ=1, 2 and 4 mm. Here we fix T_{ig}=800 K since we are interested in the response of the three-staged ignition process to mixing layer thickness. A thinner mixing layer leads to a larger scalar dissipation rate and thus is expected to prohibit the ignition process. However, Fig. 8 shows that the cool flame ignition is not affected by δ, and that only the subsequent warm and hot flame ignition is longer delayed by decreasing δ. This is because the cool flame is directly ignited by the hot spot in a very short time and thereby it is not sensitive to the dissipation rate. As shown

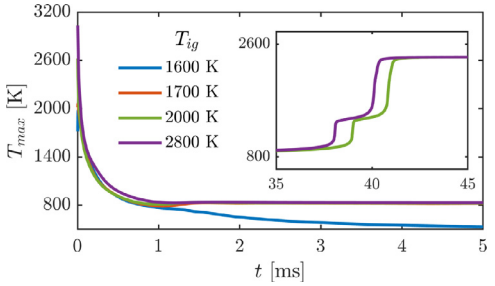

Fig. 9. Temporal evolution of $T_{\max}$ for different hot spot temperatures, T_{ig}, and fixed r_{ig}=0.25 mm, δ=2 mm, T_0=450 K and P_0=5 atm.

in the enlarged insert in Fig. 8, the $T_{\max}$ histories for cool flames ignited in mixing layers with different δ agree well with that from the 0D homogeneous ignition with ϕ=3.82 (i.e., Z=0.3). This further indicates that the cool flame ignition in the mixing layer is analogous to the ignition in the homogeneous system. In contrast, the warm flame is initiated through the auto-ignition of the products of the cool flame after a relatively long period of time (>20 ms). Consequently, the accumulation of heat and radicals for ITC is greatly influenced by the dissipation rate. Nevertheless, Fig. 8 shows that the duration between warm flame ignition and hot flame ignition is not sensitive to δ. This is because this duration is mainly determined by the propagation of the warm flame and the time it takes to reach the stoichiometric plane.

To assess the effects of hot spot radius (also termed as spark gap distance in [13,18]), the default value r_{ig}=0.5 mm is halved to r_{ig}=0.25 mm here. The resulting temporal evolutions of $T_{\max}$ are plotted in Fig. 9 for different T_{ig}. It is found that no hot flame can be directly initiated even at T_{ig}=2800 K. Instead, there exists a critical hot spot temperature T_c between 1600 K and 1700 K for cool flame ignition. When $T_{ig} > T_c$, a cool flame is ignited and subsequently warm and hot flames are developed after a period of time as shown in the insert in Fig. 9. This phenomenon can be explained through the mixture fraction region covered by the hot spot. In the previous simulations where r_{ig}=0.5 mm is used, the hot spot spans over a wide range in mixture fraction space with $0.08 < Z < 0.92$ which covers both the most reactive mixture fraction (Z=0.3) and the stoichiometric mixture fraction (Z_{st}=0.1), and thus a hot or a cool flame can be directly ignited depending on T_{ig} as shown in Fig. 2b. However, for r_{ig}=0.25 mm, the mixture fraction range covered by the hot spot is $0.24 < Z < 0.76$ which only covers the most reactive mixture fraction but not the stoichiometric mixture fraction. Consequently, only a cool flame is directly ignited.

The above results indicate that the mixture fraction range covered by the hot spot has a strong impact on subsequent flame initiation. The mix-

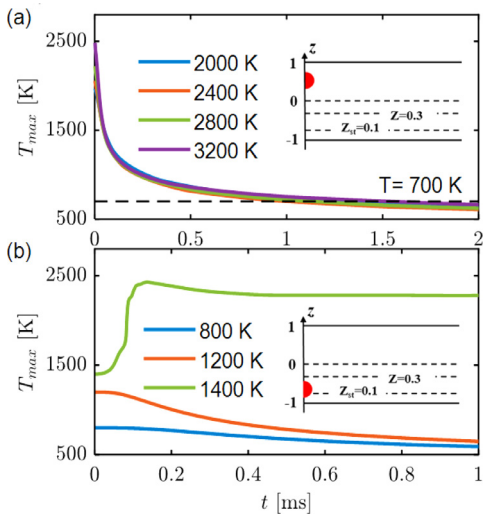

Fig. 10. The temporal evolution of $T_{\max}$ for different hot spot temperatures, T_{ig}, and fixed r_{ig}=0.25 mm, T_0=450 K and P_0=5 atm. The insert shows that the hot spot is placed 0.5 mm above (a) and below (b) the central horizontal line.

ture fraction range within the hot spot can also be changed by changing the hot spot position. The results for different hot spot positions are shown in Fig. 10. Figure 10a shows that placing the hot spot 0.5 mm above the central horizontal line covering neither the Z=0.3 plane nor Z_{st}=0.1 plane, $T_{\max}$ decreases with time in all cases and no flame can be ignited. In contrast, Fig. 10b shows that placing the hot spot 0.5 mm below the central horizontal line covering the Z_{st}=0.1 plane, only the hot flame can be ignited.

Therefore, different ignition modes (e.g., no flame initiation, only hot flame initiation and only cool flame initiation) can be achieved via changing the temperature, size and position of the hot spot. The hot spot configuration has a significant impact on forced ignition in non-premixed reactants. In this context, it is expected that in turbulent flows different ignition modes could be augmented when LTC is considered.

3.4. Cool flame dynamics in the mixing layer

Figure 3 indicates the duration of the cool flame for more than 20 ms before it is merged by the warm flame. Besides, the cool flame has reached a quasi-steady state as it propagates along the Z=0.3 isoline with quasi-constant $T_{\max}$ and $S_{d,\max}$. Therefore, we can study the propagation properties of cool flames in the mixing layer.

The propagation mode of the cool flame can be identified by comparing the contributions of the reaction term and diffusion term in the energy balance equation. To this end, the displacement speed, S_d, is decomposed into two components, $S_{d,rec}$ and

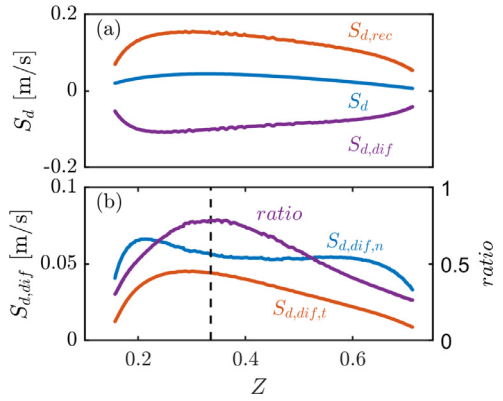

Fig. 11. The distributions of (a) S_d and its two components and (b) $|S_{d,dif,n}|$ and $|S_{d,dif,t}|$ as well as their ratio $|S_{d,dif,t}|/|S_{d,dif,n}|$ in Z space for t=20 ms, T_{ig}=800 K, T_0=450 K and P_0=5 atm. The dashed line denotes the position where the flame curvature is maximum.

$S_{d,dif}$, which correspond to the contributions of chemical reactions and thermal diffusion, respectively. From the RHS of Eq. (3), $S_{d,rec}$ and $S_{d,dif}$ can be extracted as:

$$S_{d,rec} = \frac{\dot{\omega}'_T}{\rho C_p |\nabla T|}, \tag{5}$$

$$S_{d,dif} = \frac{\nabla \cdot (\lambda \nabla T)}{\rho C_p |\nabla T|}, \tag{6}$$

The propagation mode can be characterized by the ratio between $S_{d,rec}$ and $S_{d,dif}$. It is a self-sustained deflagration wave (diffusion-driven) if $S_{d,dif}$ is in the same order of magnitude as $S_{d,rec}$ while it is a spontaneous ignition front (reaction driven) if $S_{d,rec}$ is dominant over $S_{d,dif}$ [4]. Figure 11a plots the distributions of $S_{d,rec}$ and $S_{d,dif}$ as well as S_d along the cool flame front as a function of mixture fraction at the same time and conditions as those in Fig. 4. It is seen that $S_{d,dif}$ is opposite in sign but comparable in magnitude with $S_{d,rec}$, indicating that the cool flame observed in Fig. 4 is a self-sustained flame front that is driven by the balance between ignition and diffusion processes.

On the other hand, from the point view of flame modeling, it is of interest to quantitatively compare the contributions of normal diffusion and tangential diffusion to the total diffusion term [28]. For this purpose, $S_{d,dif}$ is further decomposed into two components as $S_{d,dif} = S_{d,dif,n} + S_{d,dif,t}$ as follows:

$$S_{d,dif,n} = \frac{\vec{n} \cdot \nabla(\lambda \vec{n} \cdot \nabla T)}{\rho C_p |\nabla T|}, \tag{7}$$

$$S_{d,dif,t} = \frac{\lambda \kappa}{\rho C_p}, \tag{8}$$

where $\kappa = \nabla \cdot \vec{n}$ is flame curvature and $\vec{n} = -\nabla T/|\nabla T|$ is unit vector of a temperature iso-surface. Equations (7) and (8) correspond

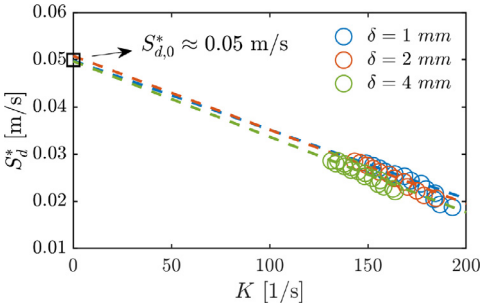

Fig. 12. The correlation of S^*_d with K for different mixing layer thickness, δ. T_{ig}=800 K, T_0=450 K and P_0=5 atm. The symbols denote simulation results. The dashed lines stand for linear fitting.

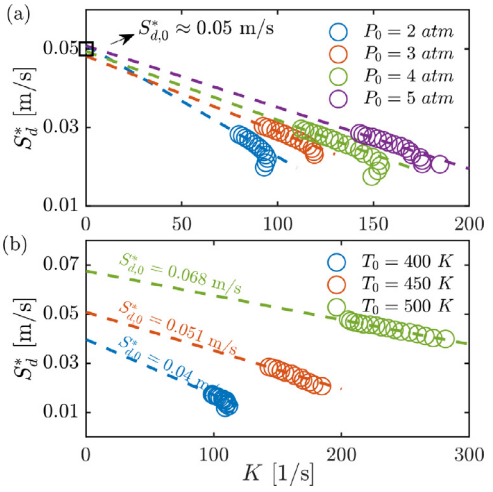

Fig. 13. Change of S^*_d with K at (a) different pressures P_0 but fixed T_0=450 K and (b) different initial temperatures T_0 but fixed P_0=5 atm for T_{ig}=800 K, r_{ig}=0.5 mm, δ=2 mm. The symbols denote simulation results. The dashed lines stand for linear fitting.

to the contributions from normal diffusion and tangential diffusion, respectively. Figure 11b plots the distributions of the absolute values of $S_{d,dif,n}$ and $S_{d,dif,t}$ as well as the ratio between $S_{d,dif,t}$ to $S_{d,dif,n}$ in mixture fraction space. In general, $S_{d,dif,t}$ is smaller than $S_{d,dif,n}$ and thus the ratio is less than 1. Nevertheless, the tangential diffusion could play a significant role, as the ratio has a minimum of 0.3 at two flame wings and has a maximum of 0.8 at flame tip where the flame curvature is maximum. Overall, Fig. 11 demonstrates that the cool flame ignited by the hot spot in the mixing layer is a self-sustained partially premixed flame and the 1D premixed or non-premixed flamelet model probably is not sufficient to characterize the multi-regime cool flame structure observed here.

Furthermore, the dependence of the cool flame propagation speed on flame stretch K is shown in Fig. 12. Here the flame stretch K is computed as $K = \nabla_t \cdot \vec{u}_t + S_d\kappa$ where ∇_t represents the gradient along the tangential direction. Note that we use the density weighted displacement speed, $S^*_d = S_{d,\max} * \rho/\rho_u$, where ρ is the local density at the location where $S_{d,\max}$ is evaluated and ρ_u is the unburnt gas density of the DME-air mixture at ϕ=3.82 (i.e., Z=0.3). Since the cool flame observed in this study propagates mainly along the Z=0.3 surface in all cases (see section S3 in Supplementary Material), the same value of ϕ=3.82 is used to compute ρ_u in all cases. Interestingly, a very good linear relationship between S^*_d and K is observed, which is consistent with previous studies for premixed cool flames [9] and for conventional triple flames [16]. Therefore, the unstretched density weighted displacement speed $S^*_{d,0}$ can be obtained from the linear extrapolation, in which the lower limit stretch rate corresponds to the instant that is about 1 ms before the occurrence of warm flame while the upper limit stretch rate was chosen so that the data as much as possible was used. Specifically, the upper limits with K=170, 160 and 140 s^{-1} were used for δ=1, 2 and 4 mm in Fig. 12. Overall, these linear fittings have very good performance with correlation coefficients higher than 0.99. Besides, it is found that the impact of mixing layer thickness on the cool flame speed is marginal and we have $S^*_{d,0} \approx$ 0.05 m/s for all δ. This is also consistent with the results for hydrogen triple flames reported in [19].

Finally, the influence of initial temperature T_0 and pressure P_0 on the $S^*_d - K$ curve is shown in Fig. 13. It is seen that the linear relationship between S^*_d and K is maintained for all cases, implying that the linear relationship is an intrinsic characteristic for cool flames propagating in the mixing layer. Moreover, it is found that P_0 has a significant impact on the Markstein length (i.e., the slope of $S^*_d - K$ curve), whereas it has a negligible influence on $S^*_{d,0}$. As for T_0, it exerts a considerable influence on both the Markstein length and $S^*_{d,0}$: a higher T_0 leads to a lower Markstein length and a larger $S^*_{d,0}$. Therefore, the cool flame speed increases with the initial temperature but is insensitive to pressure change. Similar trend was also reported in [7].

4. Conclusions

In this study, a series of two-dimensional simulations for forced ignition in a quiescent DME-air mixing layer are conducted. The emphasis is placed on assessing the effects of LTC on the evolution of the ignition kernel in non-premixed mixtures.

The results show that under elevated temperatures and pressures, a cool flame or a warm flame can be directly ignited depending on the hot spot temperature. When a relatively low hot spot temperature is applied, a three-staged ignition process

is observed where the cool, warm and hot flames are initiated sequentially, leading to a trailing warm flame and a trailing cool flame attached to a hot triple flame in the very rich region. To the best of our knowledge, this penta-brachial flame structure has not been reported in the literature. Moreover, it is found that the formation of the penta-brachial flame structure is attributed to the LTC and ITC.

Furthermore, a parametric study is performed to understand the impact of the mixing layer thickness δ and hot spot configuration (i.e., size and position) on ignition kernel development. It is found that, while the cool flame ignition is not sensitive to the change in δ, the subsequent warm flame or hot flame initiation can be significantly delayed by decreasing δ due to increased dissipation rate. Moreover, it is demonstrated that the mixture fraction range covered by the hot spot has a great impact on subsequently flame initiation. Different ignition modes (e.g., no flame initiation, only hot flame initiation and only cool flame initiation) can be achieved via changing the temperature, size and position of the hot spot.

The characteristics of cool flame propagation are also investigated. The cool flame in the mixing layer is found to be a self-sustained partially premixed flame. Its density-weighted displacement speed changes linearly with flame stretch. The unstretched cool flame speed increases with the initial temperature but is not sensitive to pressure change. The Markstein length of cool flame strongly depends on both the initial temperature and pressure.

The present results open up the possibility of employing local low-temperature hot spots to facilitate ignition. This work is a first step towards a better understanding of how LTC affects nonpremixed ignition and thereby a simple static mixing layer is considered. In future works, it would be interesting to consider complex flow configurations.

Declaration of Competing Interest

The authors declare that they have no known competing financial interests or personal relationships that could have appeared to influence the work reported in this paper.

Acknowledgment

This research was funded by National Natural Science Foundation of China (No. 52176096).

Supplementary material

A supplementary material is associated with this article.

Supplementary material associated with this article can be found, in the online version, at doi:10.1016/j.proci.2022.07.024.

References

[1] Y. Ju, Understanding cool flames and warm flames, Proc. Combust. Inst. 38 (1) (2021) 83–119.
[2] R.N. Dahms, G.A. Paczko, S.A. Skeen, L.M. Pickett, Understanding the ignition mechanism of high-pressure spray flames, Proc. Combust. Inst. 36 (2) (2017) 2615–2623.
[3] S. Deng, P. Zhao, M.E. Mueller, C.K. Law, Autoignition-affected stabilization of laminar nonpremixed DME/air coflow flames, Combust. Flame 162 (9) (2015) 3437–3445.
[4] A. Krisman, E.R. Hawkes, M. Talei, A. Bhagatwala, J.H. Chen, Polybrachial structures in dimethyl ether edge-flames at negative temperature coefficient conditions, Proc. Combust. Inst. 35 (1) (2015) 999–1006.
[5] A. Krisman, E.R. Hawkes, M. Talei, A. Bhagatwala, J.H. Chen, A direct numerical simulation of cool-flame affected autoignition in diesel engine-relevant conditions, Proc. Combust. Inst. 36 (3) (2017) 3567–3575.
[6] X. Zhang, C. Yuan, L. Zhou, W. Zhao, Z. Liu, H. Wei, Effects of initial temperature on ignition and flame propagation of dual-fuel mixture in mixing layer, Combust. Flame 225 (2021) 468–484.
[7] W. Zhang, M. Faqih, X. Gou, Z. Chen, Numerical study on the transient evolution of a premixed cool flame, Combust. Flame 187 (2018) 129–136.
[8] Y. Wang, H. Zhang, T. Zirwes, F. Zhang, H. Bockhorn, Z. Chen, Ignition of dimethyl ether/air mixtures by hot particles: impact of low temperature chemical reactions, Proc. Combust. Inst. 38 (2) (2021) 2459–2466.
[9] Q. Yang, P. Zhao, Minimum ignition energy and propagation dynamics of laminar premixed cool flames, Proc. Combust. Inst. 38 (2) (2021) 2315–2322.
[10] E. Mastorakos, Ignition of turbulent non-premixed flames, Prog. Energy Combust. Sci. 35 (1) (2009) 57–97.
[11] E.S. Richardson, E. Mastorakos, Numerical investigation of forced ignition in laminar counterflow non-premixed methane-air flames, Combust. Sci. Technol. 179 (1–2) (2007) 21–37.
[12] S.F. Ahmed, R. Balachandran, E. Mastorakos, Measurements of ignition probability in turbulent non-premixed counterflow flames, Proc. Combust. Inst. 31 (1) (2007) 1507–1513.
[13] S.F. Ahmed, E. Mastorakos, Spark ignition of lifted turbulent jet flames, Combust. Flame 146 (1) (2006) 215–231.
[14] N. Chakraborty, E. Mastorakos, Direct numerical simulations of localised forced ignition in turbulent mixing layers: the effects of mixture fraction and its gradient, Flow Turbul. Combust. 80 (2) (2008) 155–186.
[15] A. Wawrzak, A. Tyliszczak, A spark ignition scenario in a temporally evolving mixing layer, Combust. Flame 209 (2019) 353–356.
[16] J. Buckmaster, Edge-flames, Prog. Energy Combust. Sci. 28 (5) (2002) 435–475.

[17] H.G. Im, J.H. Chen, Structure and propagation of triple flames in partially premixed hydrogen–air mixtures, Combust. Flame 119 (4) (1999) 436–454.
[18] R. Owston, J. Abraham, Flame propagation in stratified hydrogen–air mixtures: spark placement effects, Int. J. Hydrog. Energy 34 (15) (2009) 6532–6544.
[19] R. Owston, J. Abraham, Numerical study of hydrogen triple flame response to mixture stratification, ambient temperature, pressure, and water vapor concentration, Int. J. Hydrog. Energy 35 (10) (2010) 4723–4735.
[20] P. Pearce, J. Daou, Initiation and evolution of triple flames subject to thermal expansion and gravity, Proc. Combust. Inst. 36 (1) (2017) 1431–1437.
[21] S. Xie, Z. Lu, Z. Chen, Effects of strain rate and lewis number on forced ignition of laminar counterflow diffusion flames, Combust. Flame 226 (2021) 302–314.
[22] F. Takahashi, V.R. Katta, Structure of propagating edge diffusion flames in hydrocarbon fuel jets, Proc. Combust. Inst. 30 (1) (2005) 375–382.
[23] J. Prager, H.N. Najm, M. Valorani, D.A. Goussis, Structure of n-heptane/air triple flames in partially-premixed mixing layers, Combust. Flame 158 (11) (2011) 2128–2144.
[24] H.G. Weller, G. Tabor, H. Jasak, C. Fureby, A tensorial approach to computational continuum mechanics using object-oriented techniques, Comput. Phys. 12 (6) (1998) 620–631.
[25] T. Zirwes, F. Zhang, P. Habisreuther, M. Hansinger, H. Bockhorn, M. Pfitzner, D. Trimis, Quasi-DNS dataset of a piloted flame with inhomogeneous inlet conditions, Flow Turbul. Combust. 104 (4) (2020) 997–1027.
[26] Z. Zhao, M. Chaos, A. Kazakov, F.L. Dryer, Thermal decomposition reaction and a comprehensive kinetic model of dimethyl ether, Int. J. Chem. Kinet. 40 (1) (2008) 1–18.
[27] D.G. Goodwin, H.K. Moffat, R.L. Speth, Cantera: An Object-oriented Software Toolkit for Chemical Kinetics, Thermodynamics, and Transport Processes. Version 2.3.0, Cantera Developers, Warrenville, IL, 2017.
[28] W. Han, A. Scholtissek, C. Hasse, The role of tangential diffusion in evaluating the performance of flamelet models, Proc. Combust. Inst. 37 (2) (2019) 1767–1774.